# Techno-economic assessment of 20MW floating wind turbines

Humberto Silva
humberto.silva@tecnico.ulisboa.pt

Instituto Superior Técnico, Universidade de Lisboa, Portugal

November 29, 2019

**Abstract**

The increasing energy demand, especially from renewable sources, calls for more efficient solutions. Wind turbines with higher rated power, deployed further offshore where the conditions are more favourable for energy production, will mark the future standards in the offshore industry. However, deeper waters make the use of floating platforms essential for their techno-economic feasibility. This thesis presents the upscaling of an 8MW floating offshore wind turbine to 20MW. The study is divided in three phases: estimation of the numerical accuracy of the simulations performed for the 8MW turbine to select the numerical settings for OpenFAST; scaling to a 20MW configuration and test it under several load cases; make an estimation of the levelized cost of energy for the 20MW turbine. The numerical accuracy of the 8MW model is affected by a compromise between time and computation capacity, but the results show that one can have confidence on the solution based on the settings chosen. After scaling to a 20MW configuration using classic similarity rules, the hydrostatic stability and dynamic behaviour under several load cases were tested, showing great stability. In fact, there might be margin to use a smaller platform with a less conservative approach. The techno-economic model showed that the system is still unable to compete with other sources of energy, but allows to conclude that there are ways of reducing the levelized cost of energy in the future.
**Keywords:** Floating offshore wind turbine; Numerical simulation; Numerical accuracy; Upscaling; Levelized cost of energy.

## 1. Introduction

### 1.1. Motivation

Climate change and the severe environmental consequences that the use of fossil fuels bring, allied with the increase in energy demand at an unprecedented rate, are making the world shift towards renewable and more sustainable energy sources. Wind powered energy generating devices are one of the main solutions for the problem stated.

Although, onshore installations are reaching its limit, especially in areas with high population density. This motivates the countries and investors to deploy wind turbines offshore. A number of the most relevant advantages of taking wind farms further away from the coastline are stated as follows: stronger and more steady wind; no limitation to the size of an offshore wind turbine; vast availability of sea surface and no dealing with land occupation; no dealing with noise pollution and visual impact. On the other hand, offshore wind turbines imply higher capital investment, more challenging structural design, less accessibility, higher costs related to maintenance issues and electric power transmission to shore [1]. This is why wind turbines with high rated power, from 5 to 10MW now and up to 20MW in the near future, are needed. Only this magnitude of power ratings can make offshore wind feasible, especially for floating wind turbines.

### 1.2. Offshore wind structures

Offshore wind support structures can be classified according to the depth of the installation site as: shallow water (<30 meters); transitional water (30 to 60 meters); deep water (>60 meters). This study is focused on the deploying of wind turbines in deep waters, thus the solution lies on floating structures. Figure 1 shows that as the industry goes to deeper waters, floating platforms become more economically viable than the others.

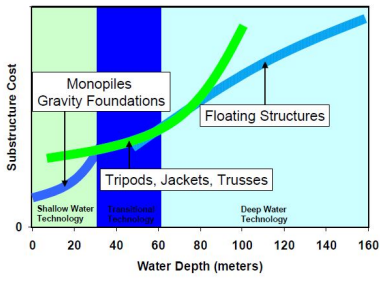


Figure 1: Variation of the cost of offshore wind substructures with water depth. [2]

Currently, there are four main types of floating platform designs: barge; semi-submersible; spar; tension-leg platform.

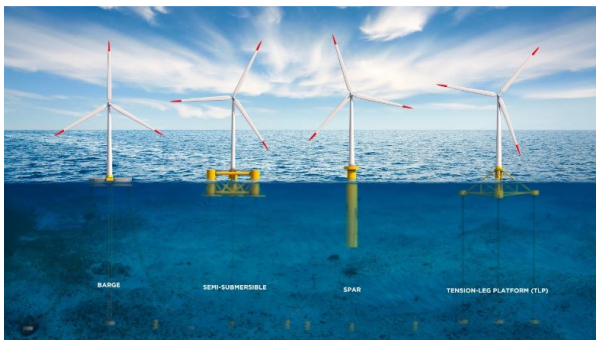


Figure 2: Main floating platform concepts. [3]

Spar and semi-submersible concepts are already proven concepts with real scale prototypes tested and pre-commercial projects ongoing, like the WindFloat Atlantic project. This study uses a semi-submersible floating platform with the WindFloat design.

### 1.3. Objectives

- Implement a model of a 8MW wind turbine identical to the WindFloat project;
- Use that model to estimate the numerical accuracy of the OpenFAST simulations and establish the numerical settings for them;
- Scale the 8MW wind turbine to 20MW and analyse its behaviour;
- Provide an estimate of the LCOE for the 20MW wind turbine.

## 2. 8MW model description

The starting point for this work is the implementation of the 8MW model in OpenFAST. Table 1 presents a general list of characteristics of the turbine.

| | |
|---|---|
| Rated electrical power | 8 MW |
| Rotor orientation | Upwind |
| Configuration | 3 blades |
| Cut-in wind speed | 4 $m/s$ |
| Cut-out wind speed | 25 $m/s$ |
| Rated wind speed | 13 $m/s$ |
| Rotor diameter | 164 $m$ |
| Hub diameter | 4 $m$ |
| Hub height | 101.75 $m$ |
| Cut-in, Rated rotor speed | 4.8, 10.5 $rpm$ |
| Rated generator speed | 500 $rpm$ |

Table 1: Vestas V164-8.0MW wind turbine general properties [4].

.

### 2.1. Nacelle and tower

The main nacelle properties needed as input for OpenFAST are presented in table 2.

| | |
|---|---|
| Length $(m)$ | 20.0 |
| Width $(m)$ | 7.5 |
| Height $(m)$ | 8.0 |
| Weight $(kg)$ | 390 000 |

Table 2: Nacelle properties.

The value used to calculate the mass per unit of length is higher than the steel density to account for some secondary structures that may be present, in this case 8500 $kg/m^3$. Table 3 presents the data that OpenFAST, through the ElastoDyn and Aerodyn modules, requires to model the tower.

| Height $(m)$ | Diameter $(m)$ | Thickness $(m)$ | Mass density $(kg/m)$ |
|---|---|---|---|
| 11.90 | 7.70 | 0.0360 | 7367.61 |
| 21.04 | 7.43 | 0.0346 | 6832.92 |
| 29.73 | 7.16 | 0.0332 | 6318.32 |
| 38.42 | 6.89 | 0.0318 | 5823.79 |
| 47.11 | 6.62 | 0.0304 | 5349.36 |
| 55.80 | 6.35 | 0.0290 | 4895.00 |
| 64.49 | 6.08 | 0.0276 | 4460.73 |
| 73.18 | 5.81 | 0.0262 | 4046.54 |
| 81.87 | 5.54 | 0.0248 | 3652.43 |
| 90.56 | 5.27 | 0.0234 | 3278.41 |
| 99.25 | 5.00 | 0.0220 | 2924.46 |

Table 3: Tower properties.

### 2.2. Rotor blades and hub

The data provided by the manufacturer about the blades is presented in table 4 [4].

| | |
|---|---|
| Rotor diameter $(m)$ | 164.0 |
| Blade length $(m)$ | 80.0 |
| Hub radius $(m)$ | 2.0 |
| Maximum chord $(m)$ | 5.4 |

Table 4: Blade data from manufacturer.

The chord at the root and tip of the blade result from an interpolation between the NREL 5MW baseline [5] and the 10MW DTU reference wind turbine [6]. The location of the maximum chord length in the blade is kept the same, in terms of percentage of its length, as in the 5MW baseline. The values between the maximum chord location and the root and tip follow a linear trend, an increase from root to maximum chord and a decrease from there to the tip. Blade twist and airfoil distribution are kept the same from the 5MW baseline model. The blade properties at root, maximum chord and tip are presented in table 5.

### 2.3. Floating platform

The floating platform consists in three columns placed in the vertices of an equilateral triangle,

| Span ($m$) | Chord ($m$) | Twist (deg) | Airfoil |
|---|---|---|---|
| 0.00 | 4.65 | 13.31 | 1 |
| 19.88 | 5.40 | 11.48 | 4 |
| 80.00 | 2.17 | 0.11 | 8 |

Table 5: Blade characteristic data for input files.

each with a hexagonal heave plate on the bottom end and with the tower placed on one fo the columns. Also, there are several braces connecting the main columns that are not modelled neither in the WAMIT simulations nor in OpenFAST, because their diameter is small when compared with the main columns. Thus, it will not have an impact on the hydrodynamics of the model, since only potential theory is used. Figure 3 is an illustration of WindFloat's floating platform.

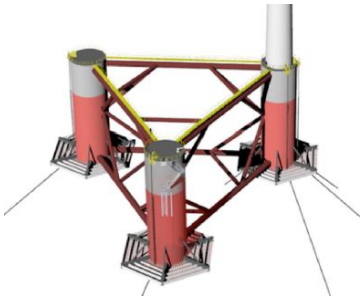

Figure 3: Three-dimensional view of the Windfloat support structure. [7]

Table 6 has the dimensions of the floating platform that were used as an input for OpenFAST's modules HydroDyn and ElastoDyn, but also to make a CAD model of the platform in SolidWorks. The CAD model was used to get the mass and moments of inertia of the platform, that are essential for the code to simulate the motion of the system.

To balance the moment crated by the wind turbine (sitting in a column, not in the platform CM) and in order to keep the operating draft (equal weight and buoyancy) as designed, the columns of the platform are filled with ballast water. The process to find the amount of ballast needed is divided in two steps, first to ensure stability and a second to keep the draft.

### 2.4. Mooring system

The floating platform is secured by three catenary mooring lines that are spread symmetrically about the platform centre of mass, as shown in figure 4.

| | | |
|---|---|---|
| Operating draft | 32.1 | $[m]$ |
| Column elevation over sea level | 11.9 | $[m]$ |
| Column centre to centre | 74.8 | $[m]$ |
| Column diameter | 13.2 | $[m]$ |
| Length of heave plate edge | 15.4 | $[m]$ |
| Heave plate thickness | 0.115 | $[m]$ |
| Column thickness | 0.0320 | $[m]$ |
| Mass (no ballast) | 2.62450E+06 | $[kg]$ |
| Ballast water (column 1) | 5976 | $[m^3]$ |
| Ballast water (columns 2 and 3) | 3488 | $[m^3]$ |
| Roll inertia | 3.18392E+09 | $[kgm^2]$ |
| Pitch inertia | 3.18392E+09 | $[kgm^2]$ |
| Yaw inertia | 5.30743E+09 | $[kgm^2]$ |

Table 6: Floating platform properties for the 8MW wind turbine.

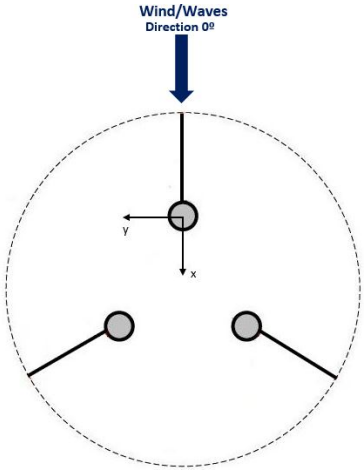


Figure 4: Sketch of the mooring system (not at scale).

Table 7 presents the most important data that OpenFAST uses as an input.

| | | |
|---|---|---|
| Number of mooring lines | 3 | [-] |
| Angle between adjacent mooring lines | 120 | [deg] |
| Water depth | 100 | $[m]$ |
| Depth from fairlead to seabed | 68.015 | $[m]$ |
| Radius to anchors from platform CM | 600 | $[m]$ |
| Radius to fairleads from platform CM | 43.18 | $[m]$ |
| Unstretched mooring line length | 566 | $[m]$ |

Table 7: Mooring configuration.

## 3. Numerical convergence properties

Most of the the mathematical models used in engineering do not have an analytical solution, this means that numerical solutions are required. OpenFAST is the code used to address this problem. As in all numerical solutions, it is not exact and there will be an error.

$$e(\phi_i) = \phi_i - \phi_{exact} \tag{1}$$

3.1. Numerical convergence

The goal of doing the verification of this code is to prove that the solution it provides does not contain significant errors. An estimate of the discretization error of a solution can be found by successively reducing the time step.

$$\phi_i = \phi_0 + \alpha h_i^p \tag{2}$$

And the error estimate for time step $i$ is:

$$e = \phi_i - \phi_0 = \alpha h_i^p \tag{3}$$

where $\phi_i$ is the approximate solution for a given time step, $\phi_0$ is the estimated value of the exact solution for the smallest time step used in the study, $\alpha$ is a constant and $p$ is the observed order of convergence [8]. In a normal mesh refinement study, $h_i$ would be the size of the mesh, but in this case is the size of the time step.

Another purpose of this work is to prove that $p$ will be equal to the theoretical order of convergence of the discretized equations. In the mesh refining study, the time step is reduced by half at each iteration, from $\Delta t = 0.1s$ until $\Delta t = 0.003125s$. So as to calculate the order of convergence and the discretization error at leat three different time steps are needed. This means that, with the six time steps used, four orders of convergence and discretization errors can be found, one for each set of three time steps.

$$\phi_3 - \phi_2 = \alpha h_2^p \left( \left( \frac{h_3}{h_2} \right)^p - 1 \right) \tag{4}$$

$$\phi_2 - \phi_1 = \alpha h_1^p \left( \left( \frac{h_2}{h_1} \right)^p - 1 \right) \tag{5}$$

$$\phi_1 - \phi_0 = \alpha h_1^p \tag{6}$$

The order of convergence is calculated by dividing equation (4) by (5). After doing some algebraic manipulation and knowing that $\frac{h_3}{h_2} = \frac{h_2}{h_1} = 2$ one gets:

$$p = \frac{\ln\left( \frac{\phi_3 - \phi_2}{\phi_2 - \phi_1} \right)}{\ln(2)} \tag{7}$$

Since the exact solution, $\phi_0$ is unknown, to get the discretization error, equation (5) is divided by (6).

$$e_1 = \phi_1 - \phi_0 = \frac{\phi_2 - \phi_1}{2^p - 1} \tag{8}$$

Once this is known, an estimate for the exact value of a variable can be calculated.

$$\phi_0 = \phi_1 - \frac{\phi_2 - \phi_1}{2^p - 1} \tag{9}$$

AeroDyn discretizes the turbine blades to implement the BEM theory, so, in order for it not to influence the choice of the time step, the aerodynamic module is disabled in this part of the study. Thus, there is only discretization in time and simulations of 300 seconds were run with an irregular sea state ($H_s = 2.5m$; $T_p = 10s$). Table 8 presents the mean displacement in heave for all the simulations done and table 9 the numerical results obtained.

| Mean | |
|---|---|
| $\Delta t$ $(s)$ | Heave $(m)$ |
| 0.1 | 0.00143 |
| 0.05 | 0.00125 |
| 0.025 | 0.00114 |
| 0.0125 | 0.00108 |
| 0.00625 | 0.00104 |
| 0.003125 | 0.00103 |

Table 8: Mean heave for each time step.

| | Heave | | | |
|---|---|---|---|---|
| i | $\phi_i - \phi_{i-1}$ | $p$ | $\phi_0$ | $e_i(\%)$ |
| 6 | 1.830E-04 | | | |
| 5 | 1.089E-04 | 0.75 | 0.00098 | |
| 4 | 6.225E-05 | 0.81 | 0.00099 | 15.92 |
| 3 | 3.340E-05 | 0.90 | 0.00101 | 8.26 |
| 2 | 1.800E-05 | 0.89 | 0.00101 | 3.85 |
| 1 | | | | 2.09 |

Table 9: Order of convergence, estimate of exact solution and discretization error for heave.

The order of convergence observed tends to a value close to one, and the explanation for it lies in the way that the code is implicitly discretizing the radiation equation with the rectangle rule, which is a first order method.

Analysing the results, one can conclude that a reasonable time step to use in the simulations to do throughout this work is 0.00625 seconds. The reason to choose this time step instead of the smallest, and consequently the one with the smaller error, lies on the fact that the simulations would become too heavy in computational terms and that would consume too much time. As a consequence, opting for the non optimal solution, but one that gives confidence in the results is a compromise that has to be done.

Afterwards, the aerodynamic module was enabled. The wave conditions are kept the same as before and a wind profile with a mean speed of $13m/s$ was generated by TurbSim. The goal now is to find the ideal number of nodes per blade of the rotor that allow the BEM method to converge. For this, a total of nine simulations were done. Firstly,

with 10 nodes per blade, three simulations with the three smaller time steps considered before. Then, the procedure was repeated for 20 and 40 nodes per blade. This allows to determine the discretization error that would be obtained for different number of nodes used.

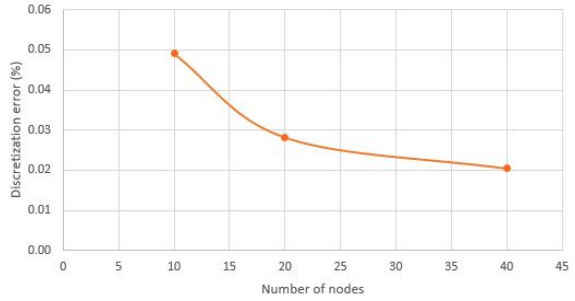


Figure 5: Error of discretization in function of the number of nodes per blade.

From figure 5, one can observe that the error of discretization is decreasing when the number of nodes per blade increases. Although the error is already very small when using 10 nodes, it is clear that there is a significant decrease when going from 10 to 20 nodes, being 57% of the error for 10 nodes, and a smaller decrease from 20 to 40 nodes. In the latter, the error of discretization is 42% of the initial error with 10 nodes. Even though the optimal solution would be to choose 40 nodes per blade, as demonstrated, it was opted to use only 20. This choice is the result of weighting time of simulation against accuracy of the results and also to the fact that the largest decrease in error arises from 10 to 20 nodes.

### 3.2. Statistical convergence

Achieving statistical convergence means that, at some point in time, the initial conditions of a simulation stop having influence over the solution in analysis. In order to do that, a very large simulation is needed, so that by the end of that period of simulated time there is no influence of the initial conditions.

In this case, a time of 2500 seconds was simulated and values of the relevant solutions were taken in periods of 500 seconds from that time series. To have consistent results, the outer factors that will have an influence on the floating structure need to be the same in each period of 500 seconds. Thus, the wave spectrum and the wind profile have to be periodic.

Table 10 displays the difference in percentage between the result taken in one period and the result of the last (2000-2500s). That is, the smaller this percentage, the less influence the initial condition still has on the solutions taken in this period.

| Mean | | | | |
|---|---|---|---|---|
| Period ($s$) | Surge | Heave | Pitch | Yaw |
| 0-500 | 19.04% | 35.53% | 2.95% | -40.91% |
| 500-1000 | 0.55% | 1.67% | -0.15% | 14.34% |
| 1000-1500 | -0.06% | -0.26% | 0.01% | 10.38% |
| 1500-2000 | 0.05% | -0.11% | 0.10% | 2.42% |
| 2000-2500 | 0.00% | 0.00% | 0.00% | 0.00% |

Table 10: Error of the mean value in each period when compared with the last $500s$.

Looking into table 10, one can see that the first period must be ruled out when taking the results from a simulation because the influence of the initial conditions is still significant. Ideally, the results would be taken from 1500 seconds, however it would no be feasible in terms of time and computational capabilities to do a 2000 seconds simulations for every case tested. So, a compromise is done. Looking at the results presented, it was opted to make simulations of 1000 seconds and take out the first 500 seconds, which allows to get confidence on the solution.

## 4. Upscaling to 20MW

The scaling procedure of the 20MW wind turbine results from the application of classical similarity rules between it and the 8MW wind turbine. So, if the power output of the wind turbine is 2.5 times bigger (from 8 to 20MW), the rotor swept area is also 2.5 times bigger, resulting in a scaling factor of:

$$sf = \sqrt{\frac{20}{8}} \simeq 1.58. \tag{10}$$

| Design parameter | Scaling factor |
|---|---|
| Linear dimensions | $sf$ |
| Power | $sf^2$ |
| Thrust at rated wind | $sf^2$ |
| Rotor mass | $sf^3$ |
| Moment of inertia of the blade | $sf^5$ |

Table 11: Scaling factors for rotor and tower parameters.

This results in the scaling factors for the rotor and tower presented in table 11 and for the platform in table 12.

| Design parameter | Scaling factor |
|---|---|
| Linear dimensions | $sf$ |
| Mass | $sf^3$ |
| Moment of inertia | $sf^5$ |
| Force | $sf^3$ |

Table 12: Scaling factors for the floating platform.

Another similarity factor needs to be accounted for when handling the rotational characteristics of the wind turbine. To ensure they are the same, the tip-speed ratio needs to be maintained constant. [9]

$$TSR = \frac{\Omega R}{V} \tag{11}$$

A summary of the characteristics of the 20MW wind turbine are presented in table 13.

| | |
|---|---|
| Rated electrical power | 20 MW |
| Rotor orientation | Upwind |
| Configuration | 3 blades |
| Cut-in wind speed | 4 $m/s$ |
| Cut-out wind speed | 25 $m/s$ |
| Rated wind speed | 13 $m/s$ |
| Rotor diameter | 259.3 $m$ |
| Hub diameter | 6.32 $m$ |
| Hub height | 159.43 $m$ |
| Rated rotor speed | 6.64 $rpm$ |
| Rated generator speed | 500 $rpm$ |

Table 13: 20MW wind turbine general properties.

4.1. Nacelle and tower

Tables 14 and 15 present all the data necessary regarding the tower and nacelle needed to run a simulation.

| | |
|---|---|
| Length $(m)$ | 31.6 |
| Width $(m)$ | 11.9 |
| Height $(m)$ | 12.6 |
| Weight $(kg)$ | 1 541 610 |

Table 14: Nacelle properties.

| Height $(m)$ | Diameter $(m)$ | Thickness $(m)$ | Mass density $(kg/m)$ |
|---|---|---|---|
| 18.82 | 12.17 | 0.0569 | 18419.0 |
| 33.27 | 11.75 | 0.0547 | 17082.3 |
| 47.01 | 11.32 | 0.0525 | 15795.8 |
| 60.75 | 10.89 | 0.0503 | 14559.5 |
| 74.49 | 10.47 | 0.0481 | 13373.4 |
| 88.23 | 10.04 | 0.0459 | 12237.5 |
| 101.97 | 9.61 | 0.0436 | 11151.8 |
| 115.71 | 9.19 | 0.0414 | 10116.3 |
| 129.45 | 8.76 | 0.0392 | 9131.1 |
| 143.19 | 8.33 | 0.0370 | 8196.0 |
| 156.93 | 7.91 | 0.0348 | 7311.2 |

Table 15: Tower properties.

4.2. Rotor blades and hub

The procedure to get the upscaled blade data was different from the other parts of the turbine. Instead of upscaling each parameter individually from the 8MW model, it was opted to use Qblade software. NREL's 5MW reference blade data comes with the code and giving the hub radius, blade length and root chord, all presented in table 16, it calculates all the discretized data needed for OpenFAST's input files.

| | |
|---|---|
| Rotor diameter $(m)$ | 259.31 |
| Blade length $(m)$ | 126.49 |
| Hub radius $(m)$ | 3.61 |
| Maximum chord $(m)$ | 7.36 |
| Root chord $(m)$ | 5.06 |

Table 16: Upscaled rotor data.

4.3. Floating platform

The floating platform geometry is kept the same as in the 8MW model. So, the same assumptions apply to this case. The only difference is that the new data is upscaled with the methodology already presented in this section.

| | | |
|---|---|---|
| Operating draft | 50.75 | $[m]$ |
| Column elevation over sea level | 18.82 | $[m]$ |
| Column centre to centre | 118.27 | $[m]$ |
| Column diameter | 20.87 | $[m]$ |
| Length of heave plate edge | 24.35 | $[m]$ |
| Heave plate thickness | 0.182 | $[m]$ |
| Column thickness | 0.032 | $[m]$ |
| Mass (no ballast) | 7.80750E+06 | $[kg]$ |
| Ballast water (column 1) | 12 085 | $[m^3]$ |
| Ballast water (columns 2 and 3) | 15 031 | $[m^3]$ |
| Roll inertia | 3.16474E+10 | $[kgm^2]$ |
| Pitch inertia | 3.16474E+10 | $[kgm^2]$ |
| Yaw inertia | 5.27183E+10 | $[kgm^2]$ |

Table 17: Floating platform properties for the 20MW wind turbine.

4.4. Mooring system

Regarding the mooring system, there are some inputs that remain the same from the 8MW model, since the mooring configuration is kept. However, the parameters regarding the platform dimensions change and also the anchor radius and unstretched mooring line length were scaled according with $sf$. All the parameters regarding the mooring configuration are shown in table 18.

| | | |
|---|---|---|
| Number of mooring lines | 3 | [-] |
| Angle between adjacent mooring lines | 120 | [deg] |
| Water depth | 100 | $[m]$ |
| Depth from fairlead to seabed | 49.432 | $[m]$ |
| Radius to anchors from platform CM | 880.39 | $[m]$ |
| Radius to fairleads from platform CM | 68.28 | $[m]$ |
| Unstretched mooring line length | 895 | $[m]$ |

Table 18: Mooring configuration.

4.5. Free decay

Before testing how the system reacts to the forces of nature, wind and waves in this case, since the presence of current is neglected, free decay tests are done. It consists in evaluating the system's response to an initial offset from the equilibrium position. Figure 6 presents the free decay response to an offset in pitch motion.

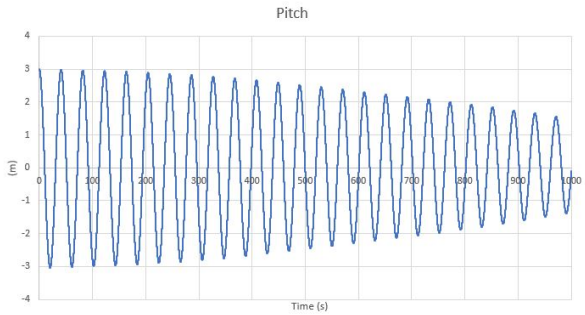


Figure 6: Pitch motion for free decay load case.

It can be seen that the motion has little damping. The fact that the effect of viscous forces is not being modelled may be causing this phenomenon. Following the methodology done by [10], for models that use potential theory without Morison elements, like this one, need extra damping to accurately represent the system's real damping. It is possible to include this extra damping coefficients trough the "additional quadratic drag" matrix in HydroDyn and they are estimated for the semi-submersible platform from OC4. However, to scale them accurately for this model is difficult due to the differences in the two geometries.

### 4.6. Constant wind

Before testing the influence that dynamic loads have on the behaviour of the system, steady state performance is tested. Figure 7 shows the mean offset in surge, but also in pitch.

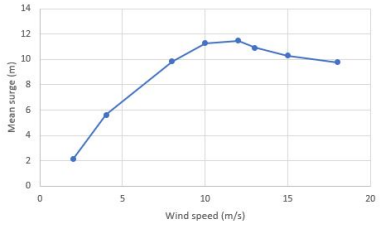


(a) Surge

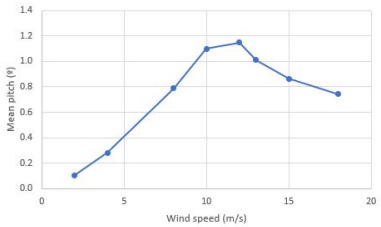


(b) Pitch

Figure 7: Mean offset of the platform.

The maximum mean value in both surge and pitch motions occurs at a wind velocity close to the rated wind speed, $12m/s$. Which is coherent with the fact that at rated wind speed there is already a blade pitch angle, that makes the thrust of the rotor become smaller. A maximum mean value of around 12 meters in surge is within an acceptable limit and a maximum of 1.15 deg as well. Actually, according to [7], the Windfloat platform designed for a 5 to 10MW wind turbine has a limit of 10 deg in operation, making this result around 10 times smaller.

### 4.7. Operational conditions

The following simulations show representative load cases of operational conditions under which the wind turbine may have to perform.

| Load case | Reference wind speed $(m/s)$ | $H_s$ $(m)$ | $T_p$ $(m)$ |
|---|---|---|---|
| 2.1 | 13 | 2 | 10 |
| 2.2 | 13 | 3 | 10 |
| 2.3 | 13 | 4 | 10 |
| 2.4 | 13 | 5 | 10 |
| 2.5 | 13 | 3 | 8 |
| 2.6 | 13 | 3 | 12 |
| 3.1 | 18 | 6 | 12 |
| 3.2 | 18 | 8 | 14 |
| 3.3 | 18 | 10 | 16 |

Table 19: Operational load cases.

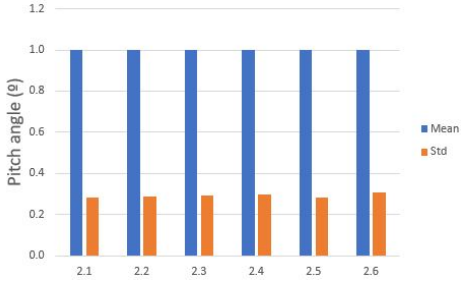


Figure 8: Mean and standard deviation of platform pitch in pre-extreme conditions.

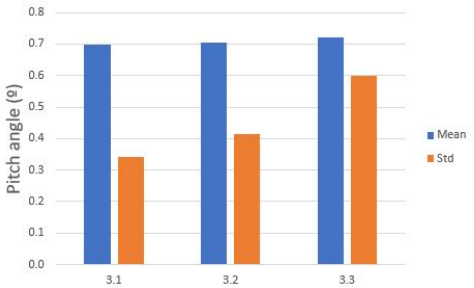


Figure 9: Mean and standard deviation of platform pitch in pre-extreme conditions.

Going through load case 3.1 to 3.3, where mean wind speed is above rated and wave conditions are rougher, one can observe in figure 9 that mean pitch is lower than in moderate conditions, illustrated in figure 8. This was expected to happen due to the blade pitch increase triggered by greater wind

speeds. Although, there is a bigger oscillation than before, as seen by the higher values of standard deviation. For load case 3.3, the standard deviation is close to the mean pitch of the platform, indicating that the pitch angle is spread over a big range of values. This case may not represent an operational condition, in a real situation this wave height would likely cause the turbine shutdown. The conditions are close to what a 50-year storm looks like [11]. Nevertheless, the simulation can be carried out by OpenFAST and the power production is ideal, producing 20MW.

## 5. Economic model

Floating wind is still in its beginnings and therefore has high costs, especially for prototypes and pre-commercial arrays, like the WindFloat Atlantic project. As the technology is still not totally developed, since there are no commercial scale projects, there is potential to reduce costs of floating wind and reach parity with fixed-bottom wind when deployed at scale.

### 5.1. Cost competitiveness level of the WindFloat technology

The Windfloat project is currently advancing with its second phase, corresponding to the deployment of three 8MW wind turbines that are schedule to operate 20 to 25 years. Thus, the TRL is level 5. Analysing figure 10, one can see that the costs are at their maximum level. However, they are expected to go down from here, so the technology should become profitable in the near future.

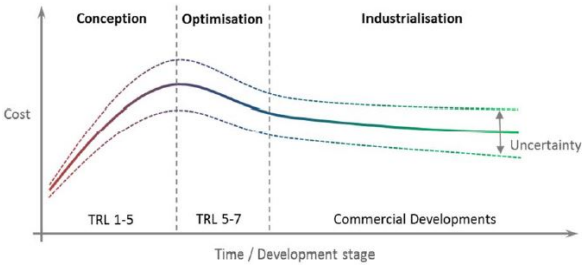


Figure 10: Cost evolution of technology through time. [12]

### 5.2. Levelized cost of energy

The levelized cost of energy measures the lifetime costs of building and operating a power generating device divided by the energy produced in its lifetime.

The project costs can be divided in categories: Capital expenditures (CAPEX); Operational expenditures (OPEX); Decommissioning costs (DECOM).

When calculating the LCOE, CAPEX and DECOM, that are one time costs, have to be depreciated over the lifetime of the project, $N$ with a discount rate , $r$. To do this, a capital recovery factor, CFR is used and it differs according to the time of the expense. If it is for a present value, such as CAPEX, equation (12) is applied, but for a future expense, like DECOM, one has to use equation (13).

$$CRF_{PV} = \frac{r(1+r)^N}{(1+r)^N - 1} \tag{12}$$

$$CRF_{FV} = \frac{r}{(1+r)^N - 1} \tag{13}$$

Knowing the annual energy production, AEP and that OPEX is an yearly payment, the LCOE can now be calculated as:

$$LCOE = \frac{CRF_{PV} \times CAPEX + OPEX + CRF_{FV} \times DECOM}{AEP} \tag{14}$$

### 5.3. Energy production

Wind availability is an important factor when calculating the cost of energy, since a wind turbine can only fulfil its purpose if the wind resource is enough. As this is an initial study, this model assumes that throughout the whole year there is a mean wind speed of 13 m/s at hub height.

The wind speed is considered to vary according to a Weibull distribution, resulting in the energy and power curves presented in figure

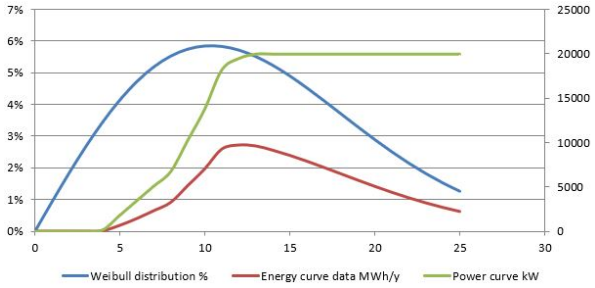


Figure 11: Relation between Weibull distribution and power and energy curves.

Considering an availability of 97% and electrical transmission losses of 4.5%, the annual energy production, AEP is 106 724 MWh, which corresponds to a 61% capacity factor.

### 5.4. Cost breakdown and results

The breakdown of the costs between CAPEX, OPEX and decommissioning is presented in table 20. Detailed information on the cost breakdown inside CAPEX and OPEX is can be consulted in [13].

With the data gathered, one can get the LCOE presented in table 21.

| **CAPEX** | $/kW | % LCOE |
|---|---|---|
| Development and management costs | 66 | 1.2% |
| Other capital project costs | 140 | 2.5% |
| Wind turbine | 1,325 | 23.4% |
| Floating Platform | 2,022 | 35.7% |
| Installation | 768 | 13.6% |
| Mooring system | 230 | 4.1% |
| Other construction costs | 217 | 3.8% |
| **Total** | **4 792** | **84.7%** |
| **OPEX** | $/kW/y | % LCOE |
| Operations | 31 | 5.0% |
| Maintenance | 62 | 9.9% |
| **Total** | **93** | **14.9%** |
| **OTHER** | $/kW | % LCOE |
| Decommissioning | 240 | 0.4% |
| **Total** | **240** | **0.4%** |

Table 20: Total breakdown of the costs.

| | $/MWh |
|---|---|
| CAPEX | 98.9 |
| OPEX | 17.4 |
| DECOM | 0.5 |
| LCOE | 116.8 |

Table 21: Simplified LCOE.

### 5.5. Factors to reduce the LCOE

The LCOE provided by this model with only one wind turbine is not competitive with the current renewable energy solutions. Table 22 gives the LCOE estimated in 2018 for onshore wind and solar energy and one can see that they are drastically inferior.

| | LCOE ($/MWh) |
|---|---|
| Onshore wind | 55 |
| Solar | 70 |

Table 22: LCOE for other technologies. [14]

One way of tackling this problem is increasing the number of devices operating in the wind farm. No project on a pre-commercial or commercial stage deploys just one wind turbine.

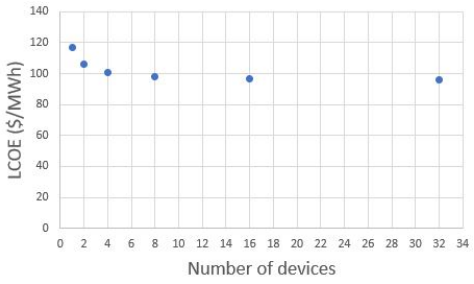


Figure 12: Variation of LCOE with the number of devices.

Figure 12 shows a decrease on the LCOE from 116.8 $/MWh to around 96 $/MWh, which is better but still not ideal. One would expect it to decrease more sharply, however it does not happen.

The model used to calculate the LCOE considers that when the number of devices increases, the OPEX keeps constant, but the CAPEX increases linearly. So, what is happening is that the LCOE will decrease until the point that the OPEX costs become negligible compared to the rest, which happens when the farm has more than 8 wind turbines.

## 6. Conclusions

This study is divided in three phases: estimation of the numerical accuracy of the simulations performed for the 8MW turbine to select the most appropriate numerical settings for the OpenFAST; scale the floating wind turbine to a 20MW configuration and test it under several load cases; make an estimate of the LCOE for the 20MW turbine.

The results obtained in this study suggest that the 20MW floating wind turbine is capable of performing under the conditions tested. Regarding the techno-economic model, it can be concluded that the cost of producing energy with a system of this magnitude can be competitive with other energy solutions in the coming years. The main conclusions from this work are listed as follows:

- An important part of this study was the estimation of the discretization error of the solutions provided by OpenFAST. This allowed to choose the settings for further simulations, such as time step, number of nodes per blade and simulation duration. It can be concluded that the optimal solution in terms of numerical error could not be chosen, because of limited time and computation resources. Nevertheless, the compromise done between accuracy of the solution and the resources gives confidence that in the solutions calculated afterwards with the settings chosen.

- Due to some geometrical uncertainties on the platform dimensions of the WindFloat Atlantic project, the dimensions used for the 8MW model are conservative. After the scaling process was done, the platform oversizing of the 8MW model shifted to 20MW platform. This has to be accounted for when analysing the response of the system to the operational load cases. For the cases 3.2 and 3.3, for wave significant heights and peak periods close to a 50-year storm, with such high mean wind speed, not only the mean pitch, but especially the standard deviation of the response should have higher values. The results obtained show that the turbine could continue to operate normally, and with significant margin, since the maximum pitch could go up to 10 degrees in a

structure of this kind. This allows to conclude that the platform has a good response under the load cases tested, but it could still perform well and be smaller, which leads to savings in terms of manufacturing and logistics and, consequently, to a smaller LCOE.

- The limitations of the economic model allow to conclude that the LCOE that was estimated can be reduced to a point where the technology might become competitive. Deploying bigger wind farms in favourable locations in terms of wind and positioning concerning the O&M logistics, together with development of more reliable technology for a turbine of such great magnitude, seem to indicate that an even lower LCOE than the one of the existing energy solutions can be achieved.

**Acknowledgements**
I would like to express my gratitude to my supervisors, Dr. Marco Alves and professor Luís Eça for their support during this project. Also, to the WavEC team for welcoming me in this period. Finally, to my family, friends and girlfriend for their support throughout this journey.

**References**

[1] Rouzbeh Siavashi. Sensitivity analysis of the dynamic response of floating wind turbines. Master's thesis, The University of Bergen, 2018.

[2] Walter Musial, Sandy Butterfield, and Bonnie Ram. Energy from offshore wind. Technical report, National Renewable Energy Lab.(NREL), Golden, CO (United States), 2006.

[3] Wind Europe. Floating offshore wind vision statement. *Wind Europe, Brussels*, 2017.

[4] Anonymous. Vestas v164-8.0mw. `https://pdf.archiexpo.com/pdf/vestas/vestas-v164-80-mw/88087-134417.html`, 2019. Accessed: 05.03.2019.

[5] Jason Jonkman, Sandy Butterfield, Walter Musial, and George Scott. Definition of a 5-mw reference wind turbine for offshore system development. Technical report, National Renewable Energy Lab.(NREL), Golden, CO (United States), 2009.

[6] Christian Bak, Frederik Zahle, Robert Bitsche, Taeseong Kim, Anders Yde, Lars Christian Henriksen, Anand Natarajan, and Morten Hartvig Hansen. Description of the dtu 10 mw reference wind turbine. *DTU Wind Energy Report-I-0092*, 5, 2013.

[7] Dominique Roddier, Christian Cermelli, Alexia Aubault, and Alla Weinstein. Windfloat: A floating foundation for offshore wind turbines. *Journal of renewable and sustainable energy*, 2(3):033104, 2010.

[8] Luís Eça. *Aerodinâmica imcompressível: Exercícios*. IST Press, 2015.

[9] Anant Jain, Amy N Robertson, Jason Mark Jonkman, Andrew J Goupee, Richard W Kimball, and Andrew HP Swift. Fast code verification of scaling laws for deepcwind floating wind system tests. Technical report, National Renewable Energy Lab.(NREL), Golden, CO (United States), 2012.

[10] Amy Robertson, Jason Jonkman, M Masciola, H Song, Andrew Goupee, Alexander Coulling, and C Luan. Definition of the semisubmersible floating system for phase ii of oc4. Technical report, National Renewable Energy Lab.(NREL), Golden, CO (United States), 2014.

[11] Amy Robertson, Jason Jonkman, Fabian Vorpahl, Wojciech Popko, Jacob Qvist, Lars Froyd, Xiaohong Chen, José Azcona, E Uzungoglu, C Guedes Soares, et al. Offshore code comparison collaboration, continuation within iea wind task 30: phase ii results regarding a floating semisubmersible wind system. Technical report, National Renewable Energy Lab.(NREL), Golden, CO (United States), 2014.

[12] Rhodri James and M Costa Ros. Floating offshore wind: market and technology review. *The Carbon Trust*, 2015.

[13] Humberto Silva. Techno-economic assessment of 20mw floating wind turbines. Master's thesis, Instituto Superior Técnico, 2019.

[14] Veronika Henze. Tumbling costs for wind, solar, batteries are squeezing fossil fuels. `https://greenbuildingelements.com/steel-building-faqs/steel-prices-forecast/`, 2018. Accessed: 16.10.2019.